Available online at www.sciencedirect.com
SCIENCE DIRECT®
Journal of Solid State Chemistry 177 (2004) 2295–2304
JOURNAL OF SOLID STATE CHEMISTRY
http://elsevier.com/locate/jssc

An electron diffraction and bond valence sum study of the space group symmetries and structures of the photocatalytic 1:2 *B* site ordered $A_3CoNb_2O_9$ perovskites ($A = Ca^{2+}$, Sr^{2+}, Ba^{2+})

V. Ting, Y. Liu, R.L. Withers,* and L. Norén

Research School of Chemistry, Australian National University, Science Road GPO Box 4, Canberra ACT 0200, Australia

Received 17 December 2003; received in revised form 2 March 2004; accepted 12 March 2004

Abstract

A careful investigation has been carried out into the space group symmetries, structures and crystal chemistries of the 1:2 *B*-site ordered triple perovskites $A_3Co^{2+}Nb_2^{5+}O_9$ ($A = Ca^{2+}$, Sr^{2+}, Ba^{2+}) using a combination of bond valence sum calculations, powder XRD and electron diffraction. A recent investigation of these compounds by Yin et al. reported a random distribution of Co^{2+} and Nb^{5+} ions onto the perovskite *B*-site positions and hence $Pm\bar{3}m$ ($a = a_p$, subscript p for parent perovskite sub-structure) space group symmetry for the $A = Ba$ and Sr compounds and a monoclinically distorted variant thereof (although no space group was given) in the case of the $A = Ca$ compound. An electron diffraction study, however, shows that the $A = Ba$ compound occurs in a 1:2 *B* site ordered trigonal $P\bar{3}m1$, $\mathbf{a}_h = \mathbf{b}_p - \mathbf{c}_p$, $\mathbf{b}_h = \mathbf{c}_p - \mathbf{a}_p$, $\mathbf{c}_h = \mathbf{a}_p + \mathbf{b}_p + \mathbf{c}_p$ structure type while both the $A = Ca$ and Sr compounds occur at room temperature in monoclinic $P12_1/c1$, $\mathbf{a}_m = [\bar{1}\bar{1}2]_p$, $\mathbf{b}_m = [1\bar{1}0]_p$, $\mathbf{c}_m = 3[110]_p$, perovskite-related structure types. The latter monclinic structure type can be described as a modulated variant of the 1:2 *B* site ordered trigonal $P\bar{3}m1$ structure type with the additional modulations associated with a $b^-b^-c^+$ octahedral tilt sequence. Bond valence sum calculations are used to explain why this should be so as well as to provide a useful zeroth-order approximation to the structures of each of the compounds.
© 2004 Elsevier Inc. All rights reserved.

Keywords: Triple perovskites; *B* site ordering; Electron diffraction and bond valence sum study

1. Introduction

$A_3^{2+}(B^{2+}M_2^{5+})O_9$ perovskites (A^{2+} = Ba, Sr, Ca; B^{2+} = Mg, Zn, Co, Ni, etc.; M^{5+} = Nb or Ta) with a 1:2 mixture of divalent and pentavalent cations on the *B* site sub-lattice representing an important sub-family of the wider cubic perovskite-related family of compounds. Various members of this 1:2 sub-family exhibit properties such as relaxor ferroelectric and piezoelectric behavior [1–2], high relative permittivity, low dielectric loss and near-zero temperature coefficients of resonant frequency [3–5]. The latter microwave dielectric properties, e.g., have led to the widespread use of 1:2 compounds such as $Ba_3ZnTa_2O_9$ as low-loss dielectrics in wireless microwave communication devices [2,6]. A further potential application was recently reported by Yin et al. [7] who found that the 1:2 $A(Co_{1/3}Nb_{2/3})O_3$ perovskites ($A = Ca^{2+}$, Sr^{2+}, Ba^{2+}) had the ability to act as visible light-driven photocatalysts.

It is known that *B*-site ordering and/or octahedral tilting can have a large effect upon the physico-chemical properties of 1:2 perovskites [2,8–12]. Tamura et al. [12], e.g., have suggested that the best dielectric properties of such compounds are associated with a fully *B* site ordered 1:2 state. It is therefore of great importance in such 1:2 systems to carefully investigate the absence or otherwise of *B* site ordering and associated structural relaxation.

In the case of the photocatalytically active $A(Co_{1/3}Nb_{2/3})O_3$ materials recently examined by Yin et al. [7], the Co^{2+} and Nb^{5+} *B*-site cations were described as "…randomly (ordered) in a charge balanced manner…", i.e., they reported random *B*-site ordering rather than the 1:2 *B* site order ([13,14]; see also Fig. 1) that might have been expected given earlier reports [14–16]. The $Ba(Co_{1/3}Nb_{2/3})O_3$ and $Sr(Co_{1/3}Nb_{2/3})O_3$ compounds were thus reported to be

*Corresponding author. Fax: 612-612-50750.
E-mail address: withers@rsc.anu.edu.au (R.L. Withers).

0022-4596/$ - see front matter © 2004 Elsevier Inc. All rights reserved.
doi:10.1016/j.jssc.2004.03.021

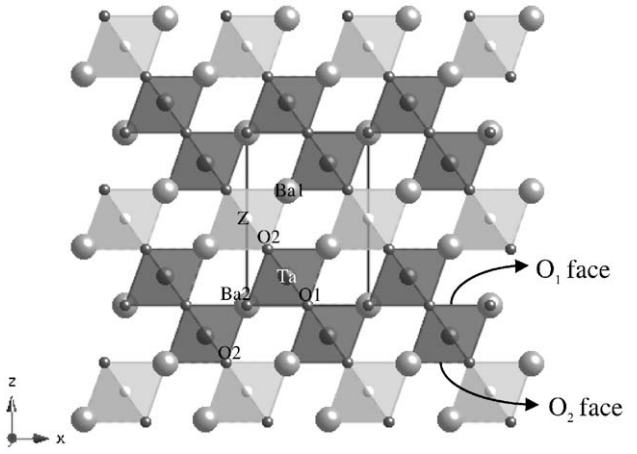

Fig. 1. Recently rerefined 1:2 *B* site ordered trigonal $P\bar{3}m1$ structure of $Ba_3ZnTa_2O_9$ (see Ref. [19]) in projection down the $\langle 010 \rangle_h$ direction. The unit cell is outlined. The smallest spheres represent O atoms, the medium spheres Zn and Ta atoms and the largest spheres the Ba ions. The light octahedra correspond to ZnO_6 octahedra while the darker octahedra correspond to TaO_6 octahedra. Note the clear 1:2 ordering scheme with alternating single layers of ZnO_6 octahedra followed by double layers of TaO_6 octahedra along the $[001]_h$ direction.

metrically cubic and of $Pm\bar{3}m$ space group symmetry ($a = a_p = 4.09$ and 3.93 Å, respectively, subscript p for the underlying perovskite parent sub-structure) while the $Ca(Co_{1/3}Nb_{2/3})O_3$ compound was reported as being metrically monoclinic [7] ($a \sim a_p = 3.911$, $b \sim a_p = 3.892$, $c \sim a_p = 3.911$ Å, $\beta = 91°16'$) although no space group was given.

Bond valence sum, or apparent valence (AV), calculations [17], on the other hand, strongly suggest that a random distribution of the *B* site cations (Co^{2+} and Nb^{5+}) is highly unlikely without major local strains occurring in the structure. In light of these ambiguities and the known sensitivity of electron diffraction to weak features of reciprocal space, a detailed electron diffraction study of the unit cells and space group symmetries of the photocatalytic $A_3CoNb_2O_9$ triple perovskites has therefore been carried out. The purpose of the current paper is to present the results of this investigation. A follow-up aim is to use a bond valence sum/group theoretical approach to understand the local crystal chemistry of these materials and thereby be able to derive a good zeroth-order model for their crystal structures.

2. Experimental

Stoichiometric ratios of BaCO3 (4 N, Aldrich), SrCO3 (5 N, Alfa) or CaCO3 (5 N, Alfa) were mixed together with Co(NO3)2 · 6H2O (97%, M&B) and Nb2O5 (>3 N, Alfa) and ground to a uniform powder under ethanol in an agate mortar. The resultant mixture was first thermally treated in an 850°C furnace for a 20 h period to drive off CO_2, then pressed into pellets and calcined at 1230°C for periods of 48 h with intermediate grinding and repelleting.

Powder samples of the fired pastilles were characterized via X-ray powder diffraction using a Guinier–Hägg XRD camera with $CuK_{\alpha 1}$ radiation to determine phase purity. Silicon (NBS No. 640) was added as an internal standard for accurate determination of the unit cell dimensions which were refined using the Unitcell software package. Transmission Electron Microscope (TEM) analysis was carried out on a Philips EM 430 TEM on crushed grains of the samples dispersed on holey carbon-coated copper grids.

3. Results and discussion

3.1. X-ray powder diffraction

The Guinier powder pattern of the $Ba(Co_{1/3}Nb_{2/3})O_3$ compound initially appeared uncomplicated with no visible evidence for splitting of any of the parent perovskite lines (although a slight broadening could be observed at high angle) or for the presence of any weak additional superstructure reflections. All of the lines could be indexed to a primitive metrically cubic unit cell with $a = 4.0836(6)$ Å, in good agreement with Yin et al. [7]. Annealing for longer periods of time than 48 h, however, resulted in the emergence of small but noticeable splittings (indicative of a lowering of the metric symmetry from cubic to hexagonal) of some parent perovskite reflections at high values of 2θ (see, e.g., Fig. 2b). Furthermore, a weak additional superstructure reflection at low angle was then observed in more heavily exposed Guinier films (see the reflection labelled $1\,0\,0_h$ in Fig. 2a). The split pattern, including the weak additional superstructure reflection, could be successfully indexed to a hexagonal, $a_h = 4.0826\sqrt{2} = 5.7737(4)$ Å, $c_h = 4.0906\sqrt{3} = 7.0852(9)$ Å (subscript h for the hexagonal Bravais lattice), unit cell.

The parent and most of the weak superstructure reflections of the $Sr(Co_{1/3}Nb_{2/3})O_3$ compound (see Fig. 2c) could also be indexed on a metrically hexagonal unit cell, with $a_h = 3.9913\sqrt{2} = 5.6445(7)$ Å, $c_h = 4.0073\sqrt{3} = 6.9408(12)$ Å. Such a cell is in reasonably good agreement with the triclinic cell reported by Treiber and Kemmler-Sack [16] ($a = b = 5.64$, $c = 6.94$ Å, $\alpha = 90.3$, $\beta = 89.7$, $\gamma = 120°$) but not with the metrically cubic 3.93 Å cell reported by Yin et al. [7]. At the highest values of 2θ there was some possible indication of even further lowering of the metric symmetry in the form of broadened lines and/or additional partial splittings of the parent perovskite lines (see, e.g., Fig. 2d). In addition, films that were exposed for 2 h clearly showed weak additional superstructure reflections not indexable on the hexagonal cell.

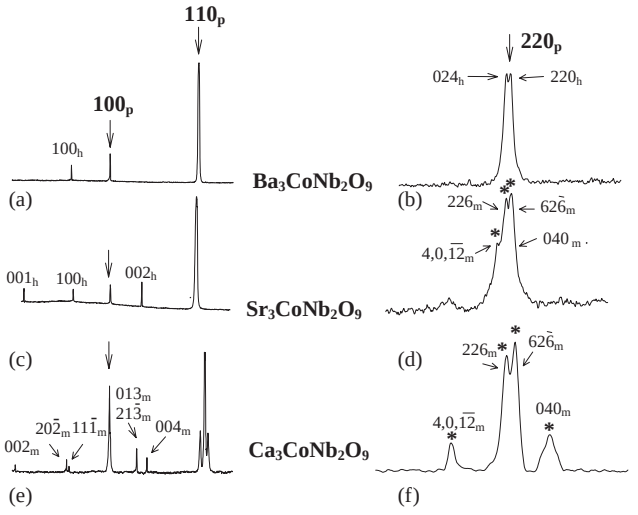

Fig. 2. Selected portions of line scans through experimental Guinier XRD patterns for each of the three $A_3CoNb_2O_9$ compounds. The lower-angle regions of the patterns (from $2\theta \sim 10°$ to $\sim 35°$ and including both the $\langle 100\rangle_p^*$ and $\langle 110\rangle_p^*$ parent reflection) are shown in (a), (c) and (e) on the left for each of the A = Ba, Sr and Ca compounds, respectively. A higher-angle region of these patterns (centered on the $\langle 220\rangle_p^*$ reflections therein) highlighting the increased splitting of the parent perovskite reflections as the A-cation size decreases is shown in (b), (d) and (f), respectively. For the indexation notation see the main text.

The pattern could be fully indexed to a monoclinic (subscript m) $\mathbf{a}_m = [\bar{1}10]_h = [\bar{1}\bar{1}2]_p$, $\mathbf{b}_m = [\bar{1}\bar{1}0]_h = [1\bar{1}0]_p$, $\mathbf{c}_m = [1\bar{1}2]_h = 3[110]_p$ supercell, with $a_m = 9.7828(7)$ Å, $b_m = 5.6429(5)$ Å, $c_m = 16.980(2)$ Å, $\beta_m = 125.205(7)°$. Just such a monoclinic perovskite-related supercell has also very recently been reported for a 1:2 ordered polymorphic form of $Ca_4Nb_2O_9$ [3,9] and for 1:2 ordered $La_3LiTi_2O_9$ [13]. (The corresponding perovskite-type parent sub-structure cell dimensions and angles derived from this monoclinic supercell are given by $a_p = b_p = 3.9962$ Å, $c_p = 3.9967$ Å, $\alpha_p = \beta_p = 89.8979°$, $\gamma_p = 89.8273°$. Note the very slight deviation from cubic metric symmetry.)

The XRD pattern of the $Ca(Co_{1/3}Nb_{2/3})O_3$ compound was by far the most complicated, showing clear parent perovskite line splittings as well as a multitude of additional superstructure reflections (see Figs. 2e and f). The parent reflections could be roughly indexed on a distorted "cubic" unit cell ($a = b = 3.9146(3)$ Å, $c = 3.8973(3)$ Å, $\gamma = 91.376(6)°$ or $180-91.376(6)° = 88.624(6)°$) in reasonable agreement with Yin et al. [7]. The pattern could, however, be fully indexed with respect to a monoclinic (subscript m) $\mathbf{a}_m = [\bar{1}\bar{1}2]_p$, $\mathbf{b}_m = [1\bar{1}0]_p$, $\mathbf{c}_m = 3[110]_p$ supercell, with $a_m = 9.5985(6)$ Å, $b_m = 5.4685(4)$ Å, $c_m = 16.8094(9)$ Å, $\beta_m = 125.719(4)°$. (The corresponding perovskite-type parent sub-structure cell dimensions and angles derived from this monoclinic supercell are given by $a_p = b_p = 3.9147$ Å, $c_p = 3.8965$ Å, $\alpha_p = \beta_p = 90.0030°$, $\gamma_p = 88.6066°$. Note that the clear parent perovskite line splittings observable in the case of the Ca compound are reflected in the rather larger metric distortion away from cubic metric symmetry.)

3.2. Electron diffraction

3.2.1. $Ba(Co_{1/3}Nb_{2/3})O_3$

Fig. 3 shows typical (a) $[001]_h$ and (b) $[100]_h$ zone axis electron diffraction patterns (EDPs) of $Ba(Co_{1/3}Nb_{2/3})O_3$ indexed both with respect to the underlying perovskite parent unit cell (subscript p) and with respect to a trigonal $P\bar{3}m1$, $\mathbf{a}_h = \mathbf{b}_p - \mathbf{c}_p$, $\mathbf{b}_h = \mathbf{c}_p - \mathbf{a}_p$, $\mathbf{c}_h = \mathbf{a}_p + \mathbf{b}_p + \mathbf{c}_p$ ($\mathbf{a}_h^* = \frac{1}{3}[\bar{1}2\bar{1}]_p^*$, $\mathbf{b}_h^* = \frac{1}{3}[\bar{2}11]_p^*$, $\mathbf{c}_h^* = \frac{1}{3}[111]_p^*$) supercell (subscript h in Fig. 3). The presence of characteristic $\mathbf{G} \pm \frac{1}{3}[111]_p^*$ satellite reflections (see, e.g., Fig. 3b) is indicative of 1:2 B site ordering and associated structural relaxation (see Fig. 1).

The absence of $\mathbf{G} \pm \frac{1}{2}\langle 111\rangle_p^*$ or $\mathbf{G} \pm \frac{1}{2}\langle 110\rangle_p^*$ type satellite reflections in Fig. 3 rules out the possibility of rigid body octahedral rotation modes accompanying the Co/Nb ordering implied by the presence of the $\mathbf{G} \pm \frac{1}{3}\langle 111\rangle_p^*$ satellite reflections. (Note that the angle brackets here denote the set of originally symmetry equivalent modulation wave-vectors, i.e., the set of modulation wave-vectors related by the $m\bar{3}m$ point group symmetry of the ideal parent perovskite structure, e.g., $\frac{1}{2}\langle 110\rangle_p^* \equiv \frac{1}{2}[110]_p^*, \frac{1}{2}[1\bar{1}0]_p^*, \frac{1}{2}[011]_p^*, \frac{1}{2}[01\bar{1}]_p^*, \frac{1}{2}[101]_p^*, \frac{1}{2}[\bar{1}01]_p^*$ while $\mathbf{G}$ refers to the set of parent perovskite-type Bragg reflections. Square brackets here and in what follows are used when a specific modulation wave-vector is being referred to.)

Given the refined hexagonal metric symmetry, the only possible resultant space group symmetry is $P\bar{3}m1$, as expected.

3.2.2. $Ca(Co_{1/3}Nb_{2/3})O_3$

Fig. 4 shows typical (a) $[03\bar{1}]_m$, (b) $[110]_m$, (c) $[010]_m$ and (d) $[100]_m$ zone axis EDPs of $Ca(Co_{1/3}Nb_{2/3})O_3$

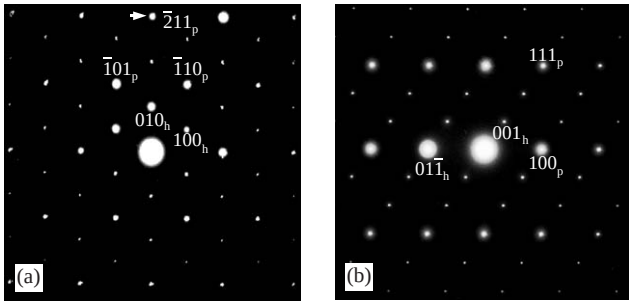

Fig. 3. (a) $[001]_h$ and (b) $[100]_h$ zone axis EDPs of $Ba(Co_{1/3}Nb_{2/3})O_3$ indexed both with respect to the underlying perovskite parent unit cell (subscript p) and with respect to a trigonal $P\bar{3}m1$, $\mathbf{a}_h = \mathbf{b}_p - \mathbf{c}_p$, $\mathbf{b}_h = \mathbf{c}_p - \mathbf{a}_p$, $\mathbf{c}_h = \mathbf{a}_p + \mathbf{b}_p + \mathbf{c}_p$ ($\mathbf{a}_h^* = \frac{1}{3}[\bar{1}2\bar{1}]_p^*$, $\mathbf{b}_h^* = \frac{1}{3}[\bar{2}11]_p^*$, $\mathbf{c}_h^* = \frac{1}{3}[111]_p^*$) supercell (subscript h).

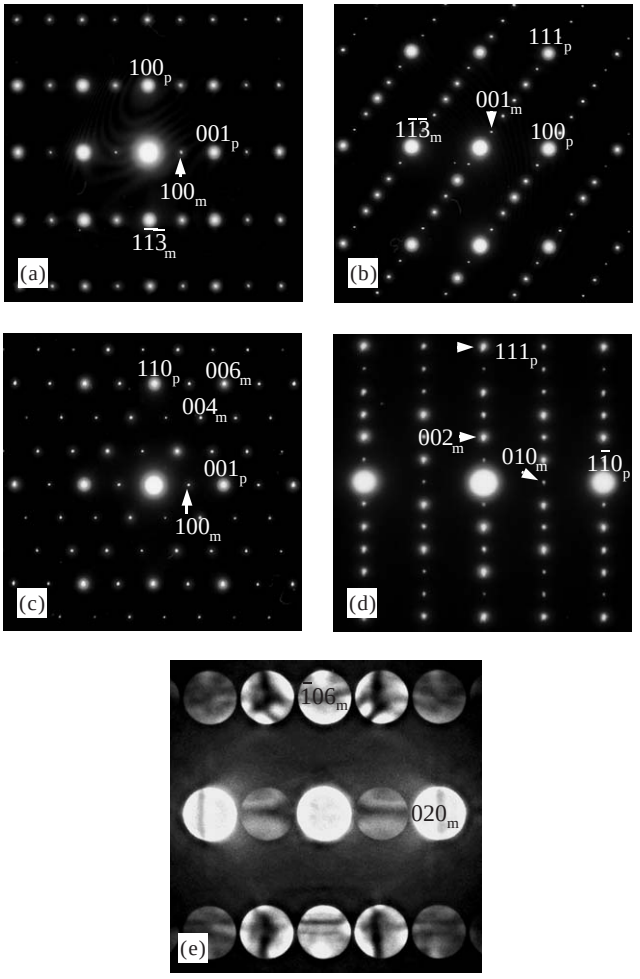

Fig. 4. Single domain (a) $[03\bar{1}]_m$, (b) $[110]_m$, (c) $[010]_m$ and (d) $[100]_m$ zone axis EDPs of $Ca(Co_{1/3}Nb_{2/3})O_3$ indexed both with respect to the perovskite parent unit cell (subscript p) and the resultant $\mathbf{a}_m = [\bar{1}\bar{1}2]_p$, $\mathbf{b}_m = [1\bar{1}0]_p$, $\mathbf{c}_m = 3[110]_p$ ($\mathbf{a}^*_m = \frac{1}{2}[001]^*_p$, $\mathbf{b}^*_m = \frac{1}{2}[1\bar{1}0]^*_p$, $\mathbf{c}^*_m = \frac{1}{6}[111]^*_p$) superstructure unit cell (subscript m).

indexed both with respect to the perovskite parent unit cell (subscript p) and the true $P2_1/c$, $\mathbf{a}_m = [\bar{1}\bar{1}2]_p$, $\mathbf{b}_m = [1\bar{1}0]_p$, $\mathbf{c}_m = 3[110]_p$ ($\mathbf{a}^*_m = \frac{1}{2}[001]^*_p$, $\mathbf{b}^*_m = \frac{1}{2}[1\bar{1}0]^*_p$, $\mathbf{c}^*_m = \frac{1}{6}[111]^*_p$) superstructure unit cell (subscript m). Given such a supercell in conjunction with the relatively close to cubic metric symmetry of the parent perovskite sub-structure, rotational twinning is only to be expected and was indeed found. For the $A = Ca$ compound, however, by contrast with the $A = Sr$ compound (see below), the size of a single domain region was quite large making it a relatively simple matter to obtain single domain EDPs. The relatively large single domain size is presumably a consequence of increased strain energy associated with twin interfaces when significant metric distortion of the underlying perovskite parent sub-structure occurs, as in the case of the $A = Ca$ compound ($a_p = b_p = 3.9147$ Å, $c_p = 3.8965$ Å, $\alpha_p = \beta_p = 90.0030°$, $\gamma_p = 88.6066°$ in the case of the Ca compound; $a_p = b_p = 3.9962$ Å, $c_p = 3.9967$ Å, $\alpha_p = \beta_p = 89.8979°$, $\gamma_p = 89.8273°$ in the case of the Sr compound). Note the presence of $\mathbf{G} \pm \frac{1}{2}[111]^*_p$ and $\mathbf{G} \pm \frac{1}{2}[1\bar{1}0]^*_p$ type satellite reflections in addition to the $\mathbf{G} \pm \frac{1}{3}[111]^*_p$ satellite reflections characteristic of 1:2 Co/Nb ordering in Fig. 4. Consequently, we can expect octahedral rotation to accompany Co/Nb ordering and associated structural relaxation in the case of the $A = Ca$ compound.

When indexed with respect to the resultant monoclinic supercell, the observed extinction conditions are: $F(h0l) = 0$ unless l is even (see Fig. 4c) and $F(0k0) = 0$ unless k is even (see Fig. 4e), necessitating a resultant monoclinic $P2_1/c$ space group symmetry. (Note that the presence of space group forbidden reflections such as $0\,0\,1_m$ in Fig. 4b and $0\,1\,0_m$ in Fig. 4d arises from dynamical diffraction and is a well-known effect in selected area EDPs where double diffraction routes into kinematically forbidden reflections exist. That $0\,0\,1_m$ is kinematically forbidden is clear from Fig. 4c where no such double diffraction routes exist. In the case of the $0\,k\,0$, k odd, reflections, the best way to confirm whether or not these reflections are kinematically forbidden is to use convergent beam electron diffraction [18]. The $[601]_m$ zone axis convergent beam EDP shown in Fig. 4e, in particular the presence of clear Gjonnes–Moodie dark bars running through the center of the $0\,k\,0$, k odd, convergent beam discs, unequivocally confirms that such reflections are kinematically forbidden [18].) Just such a supercell and space group symmetry has also recently been reported for the 1:2 ordered polymorphic form of $Ca_4Nb_2O_9$ [3,9] and for 1:2 ordered $La_3LiTi_2O_9$ [13], as mentioned above.

3.2.3. $Sr(Co_{1/3}Nb_{2/3})O_3$

In the case of the $Sr(Co_{1/3}Nb_{2/3})O_3$ compound, the rather closer to cubic metric symmetry of the underlying parent structure resulted in a typically fine scale twinned structure with domain sizes that made it rather difficult to obtain single-domain EDPs. Fig. 5a, e.g., shows a commonly obtained twinned $\langle 110 \rangle_p$ type zone axis EDP while Fig. 5b shows one of the two single domain variant EDPs making up the composite EDP of Fig. 5a. (Careful positioning of the incident electron probe with respect to the sample and a fair degree of luck is required to obtain single domain EDPs in the case of this $A = Sr$ compound.) Comparison of this single domain $[110]_m$ EDP with Fig. 4b strongly suggests that the $Sr(Co_{1/3}Nb_{2/3})O_3$ and $Ca(Co_{1/3}Nb_{2/3})O_3$ compounds are isostructural. The single domain $[301]_m$ and close to $[101]_m$ zone axis EDPs shown in Fig. 5c and d confirm the $\mathbf{a}_m = [\bar{1}\bar{1}2]_p$, $\mathbf{b}_m = [1\bar{1}0]_p$, $\mathbf{c}_m = 3[110]_p$ ($\mathbf{a}^*_m = \frac{1}{2}[001]^*_p$, $\mathbf{b}^*_m = \frac{1}{2}[1\bar{1}0]^*_p$, $\mathbf{c}^*_m = \frac{1}{6}[111]^*_p$) superstructure unit cell and is consistent with the hypothesis that the $A = Sr$ and Ca compounds are indeed isostructural.

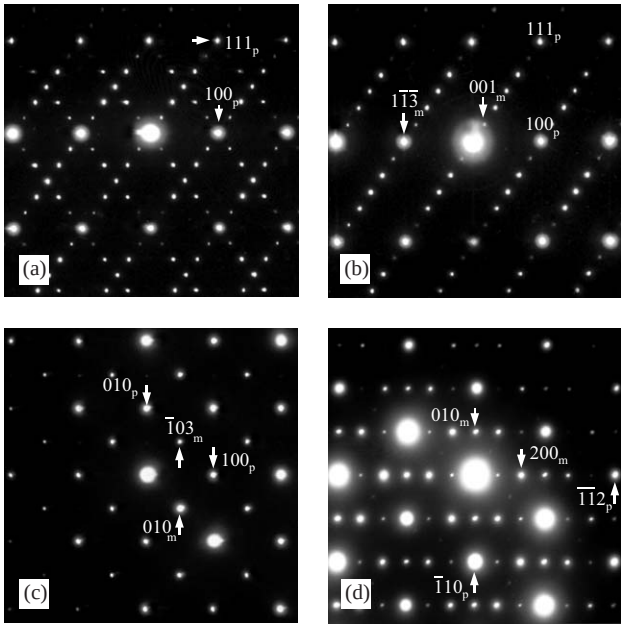

Fig. 5. Single domain (b) $[110]_m$, (c) $[301]_m$ and (d) $[101]_m$ zone axis EDPs of $Sr(Co_{1/3}Nb_{2/3})O_3$ indexed both with respect to the perovskite parent unit cell (subscript p) and the resultant $\mathbf{a}_m = [\bar{1}\bar{1}2]_p$, $\mathbf{b}_m = [1\bar{1}0]_p$, $\mathbf{c}_m = 3[110]_p$ ($\mathbf{a}^*_m = \frac{1}{2}[001]^*_p$, $\mathbf{b}^*_m = \frac{1}{2}[1\bar{1}0]^*_p$, $\mathbf{c}^*_m = \frac{1}{6}[111]^*_p$) superstructure unit cell (subscript m). (a) A twinned $\langle 110 \rangle_p$ type zone axis EDP (cf. with Fig. 4b) illustrating the extensive fine-scale twinning typical of the $Sr(Co_{1/3}Nb_{2/3})O_3$ compound.

3.3. Local crystal chemical considerations and predicted fractional co-ordinates

3.3.1. $Ba_3CoNb_2O_9$

The highest possible space group symmetry compatible with 1:2 type *B* cation ordering of an $A_3CoNb_2O_9$ triple perovskite is trigonal $P\bar{3}m1$, $\mathbf{a}_h = \mathbf{b}_p - \mathbf{c}_p$, $\mathbf{b}_h = \mathbf{c}_p - \mathbf{a}_p$, $\mathbf{c}_h = \mathbf{a}_p + \mathbf{b}_p + \mathbf{c}_p$ with Co at 0, 0, $\frac{1}{2}$; Nb at $\frac{1}{3}$, $\frac{2}{3}$, $\frac{1}{6} + \varepsilon_{Nb}$; *A*1 at $\frac{1}{3}$, $\frac{2}{3}$, $\frac{2}{3} + \varepsilon_A$; *A*2 at 0, 0, 0; O1 at $\frac{1}{2}$, 0, 0 and O2 at $(\frac{1}{6} + \varepsilon_O)$, $2(\frac{1}{6} + \varepsilon_O)$, $(\frac{1}{3} - \varepsilon'_O)$ (see, e.g., Table 5 of Ref. [19] and Fig. 1). Note that an alternative, and entirely equivalent, set of fractional co-ordinates can be obtained by adding $\frac{1}{2}$ to the above *z* fractional co-ordinates. In this setting the origin moves from the *A*2 ion to the Co ion. (We will use this setting later on when discussing the *A* = Sr and Ca compounds. These latter compounds can be described as modulated variants of an intermediate trigonal $P\bar{3}m1$ parent structure.) Given that the hexagonal unit cell parameters are fixed at the values found by powder XRD above, there remain four structural degrees of freedom, ε_O, ε'_O, ε_{Nb} and ε_A, to be adjusted in order to satisfy as closely as possible the bond valence sum requirements [17] of the six independent ions per $P\bar{3}m1$, 1:2 *B* site ordered unit cell.

If each of these four adjustable parameters are put to zero, fractional co-ordinates appropriate to an ideal perovskite parent structure (in a trigonal $P\bar{3}m1$ setting) result. Bond valence sum, or AV, calculations [17] for $Ba_3CoNb_2O_9$ in this limit give ~16% under-bonded Nb ions, ~16% over-bonded Co ions, Ba1 and Ba2 ions each over-bonded by ~19%, O1 ions over-bonded by 10% and O2 ions under-bonded by ~6% (see column 2 of Table 1). Clearly, the CoO_6 octahedra need to expand and the NbO_6 octahedra need to contract whilst the initial cuboctahedral Ba–O separation distances of the perovskite parent structure, on the other hand, need to be maintained as far as possible in order to avoid increasing the already significant over-bonding of one or other of the two Ba ions even further. In terms of the above $P\bar{3}m1$ allowed fractional co-ordinates, this requires that $\varepsilon_O = \varepsilon'_O$ and positive while $\varepsilon_A = 0$.

Table 1
Calculated AVs for the six independent ions of the $P\bar{3}m1$ $Ba_3CoNb_2O_9$ compound for both the ideal (undistorted) parent perovskite structure (column 2) as well as for the final predicted structure ($\varepsilon_O = \varepsilon'_O = 0.0077$, $\varepsilon_{Nb} = 0.0090$; column 3)

Atom label	Parent AV	Calculated result ($\varepsilon_O = \varepsilon'_O = 0.0077$, $\varepsilon_{Nb} = 0.0090$)			
		AV	Fractional co-ordinates		
			x	*y*	*z*
Co	2.326	1.802	0.0000	0.0000	0.5000
Nb	4.204	4.890	0.3333	0.6667	0.1757
Ba1	2.379	2.371	0.3333	0.6667	0.6667
Ba2	2.379	2.375	0.0000	0.0000	0.0000
O1	2.194	2.059	0.5000	0.0000	0.0000
O2	1.881	2.087	0.1744	0.3487	0.3256

The predicted fractional co-ordinates are also given in the latter case (columns 4–6).

This $\varepsilon_O = \varepsilon'_O$ positive requirement, when coupled with the further $\varepsilon_A = 0$ assumption, not only ensures that each O2 ion moves directly away from its nearest neighboring Co ion and directly towards its nearest neighboring Nb ion (thus leading to the crystal chemically necessary expansion in size of the CoO_6 octahedra and associated contraction of the NbO_6 octahedra) but also that each O2 ion moves orthogonally with respect to each of its four nearest neighbor bonds to *A* ions (thus maintaining the ideal cuboctahedral Ba–O separation distances of the perovskite parent structure and not increasing even further the already ~19% over-bonding of the Ba ions on the *A*1 and *A*2 sites). Note that the latter over-bonding of the Ba ions on the *A*1 and *A*2 sites cannot be remedied by the remaining ε_{Nb} displacive shift either. Consequently, one would not expect, and one does not observe (see Fig. 3), condensed octahedral rotation modes in the *A* = Ba case. Such octahedral rotation could only increase even further the initial ~19% over-bonding of the Ba ions on the *A* sites.

Now because the O1 ion is typically over-bonded while the Nb and O2 ions are typically under-bonded with the ideal parent perovskite fractional co-ordinates

(see column 2 of Table 1), the Nb ions are repelled away from the O1 octahedral face and towards the incoming O2 octahedral face (see Fig. 1) leading to off-centered Nb co-ordination polyhedra (see also Ref. [13]). Local crystal chemistry thus dictates that each of the parameters, ε_O ($\sim\varepsilon'_O$) and ε_{Nb}, should necessarily be positive. It is interesting to note that the often quoted neutron powder diffraction refinement of the crystal structure of $Ba_3ZnTa_2O_9$ (see Table 3 of Ref. [20]), despite the apparently quite reasonable refinement statistics, etc., had the wrong sign for each of these parameters. The relative insensitivity of powder diffraction data to the sign of small amplitude shift parameters is known but perhaps not appreciated enough. The obvious mistake in this particular case has only very recently been recognized and corrected [19].

In order to obtain a plausible magnitude for ε_O ($=\varepsilon'_O$) and ε_{Nb}, minimization of the valence least squares (VLS) functional [21]

$$\Delta = \sum_i n_i[\Delta(\mathrm{AV})_i]^2 \qquad (1)$$

has been used, where the summation is over the six crystallographically independent sites per $P\bar{3}m1$ unit cell, n_i represents the multiplicity of that site and $\Delta(\mathrm{AV})_i$ represents the deviation in calculated bond valence sum or AV from the ideal valence for site i [17]. (It should be noted that similar methods of VLSs minimization are implemented in the program SPUDS [22] and used to predict octahedral rotation magnitudes and resultant fractional co-ordinates in some perovskite-related structures. To date, however, the program is not well adapted for the triple perovskites discussed in the current contribution.) The ideal perovskite, initial value of this functional is 2.002, equivalent to an average mean square deviation $\Delta\mathrm{AV} = \sqrt{(\sum_i n_i[\Delta(\mathrm{AV})_i]^2/\sum_i n_i)}$ of ~ 0.365.

We have systematically investigated the behavior of Δ as a function of ε_O ($=\varepsilon'_O$) and ε_{Nb} by varying ε_O as a function of a fixed ε_{Nb} (see Fig. 6a). In each case a clear minimum was found with the overall minimum occurring in the close vicinity of ε_O ($=\varepsilon'_O$) ~ 0.0077 and $\varepsilon_{Nb} \sim 0.0090$. The minimum value of the functional at this position, $\Delta = 0.535$, corresponds to a much improved average mean square deviation in AV, $\Delta(\mathrm{AV}) = \sqrt{(\sum_i n_i[\Delta(\mathrm{AV})_i]^2/\sum_i n_i)}$, of ~ 0.189. The six individual $n_i[\Delta(\mathrm{AV})_i]^2$ contributions to Δ as a function of ε_O for $\varepsilon_{Nb} = 0.0090$ are shown in Fig. 6b. Note that the major contribution to $\Delta(\sim 0{\cdot}45)$ arises from the contributions of the over-bonded Ba ions. Substitution of the bond valence sum suggested values for ε_O ($=\varepsilon'_O$) $= 0.0077$ and $\varepsilon_{Nb} = 0.0090$ into the above given general fractional co-ordinate positions should thus lead to a pretty good zeroth-order approximation to the resultant structure of $Ba_3CoNb_2O_9$ (see columns 4–6 of Table 1).

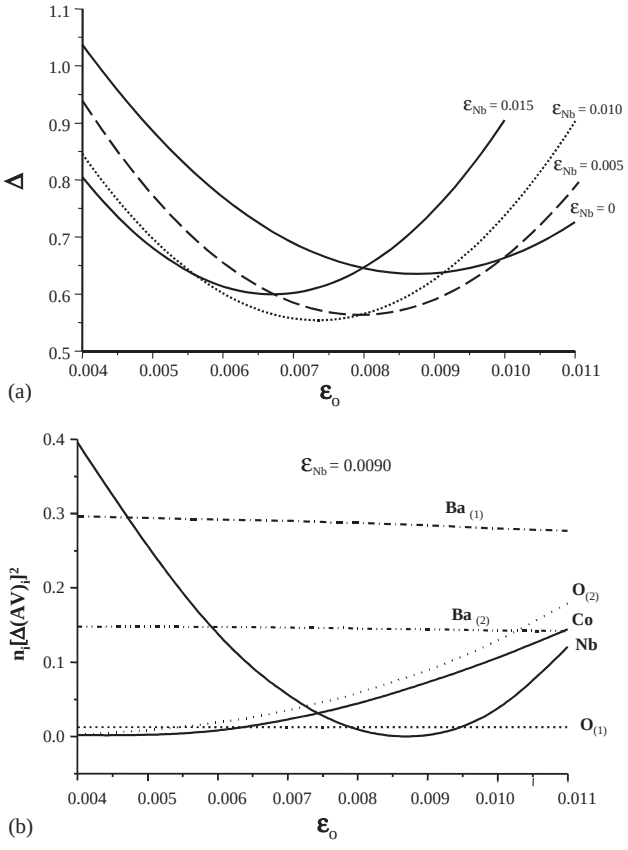

Fig. 6. (a) A plot of $\Delta = \sum_i n_i[\Delta(\mathrm{AV})_i]^2$ as a function of ε_O ($=\varepsilon'_O$) for $\varepsilon_{Nb} = 0, 0.005$, 0.010 and 0.015. In each case a clear minimum occurs. The overall minimum is found to occur in the close vicinity of ε_O ($=\varepsilon'_O$) ~ 0.0077 and $\varepsilon_{Nb} \sim 0.0090$. The six individual $n_i[\Delta(\mathrm{AV})_i]^2$ contributions to Δ as a function of ε_O for $\varepsilon_{Nb} = 0.0090$ are shown in (b).

3.3.2. $Sr_3CoNb_2O_9$ and $Ca_3CoNb_2O_9$

In the cases of $Sr_3CoNb_2O_9$ and $Ca_3CoNb_2O_9$, however, the situation is fundamentally different as a result of the significantly smaller size of the A cations. In addition to the degrees of freedom associated with 1:2 B site ordering and accompanying structural relaxation described above, we also have to take into account the extra structural degrees of freedom associated with octahedral rotation and the consequent overall symmetry lowering (from trigonal $P\bar{3}m1$, $\mathbf{a}_h = \mathbf{b}_p - \mathbf{c}_p$, $\mathbf{b}_h = \mathbf{c}_p - \mathbf{a}_p$, $\mathbf{c}_h = \mathbf{a}_p + \mathbf{b}_p + \mathbf{c}_p$, to monoclinic $P12_1/c1$, $\mathbf{a}_m = [\bar{1}10]_h = [\bar{1}\bar{1}2]_p$; $\mathbf{b}_m = [\bar{1}\bar{1}0]_h = [1\bar{1}0]_p$; $\mathbf{c}_m = [1\bar{1}2]_h = 3[110]_p$).

In order to understand the crystal chemical origin of the observed symmetry lowering (cf., e.g., Fig. 3 with Figs. 4 and 5), consider a hypothetical intermediate trigonal $P\bar{3}m1$ structure for the A = Sr and Ca cases. In the A = Sr case, e.g., using the XRD refined hexagonal cell dimensions and choosing ε_O ($=\varepsilon'_O$) ~ 0.00627 and $\varepsilon_{Nb} \sim 0.0100$ gives 7% over-bonded Co and Nb ions, 11.65% under-bonded Sr ions and O ions that are essentially happily bonded (see column 2 of Table 2).

Table 2
Bond valence sum calculations for hypothetical $P\bar{3}m1$, $Sr_3CoNb_2O_9$ and $Ca_3CoNb_2O_9$ using $a_h = b_h \sim 5.6445$, $c_h \sim 6.9408$ Å, $\varepsilon_O = \varepsilon'_O \sim 0.00627$, $\varepsilon_{Nb} \sim 0.0100$ for A = Sr and $a_h = b_h \sim 5.5498$, $c_h \sim 6.7203$ Å, $\varepsilon_O = \varepsilon'_O \sim 0.0064$, $\varepsilon_{Nb} \sim 0.0102$ for A = Ca

Atom label	AV (A = Sr) $\varepsilon_O = \varepsilon'_O$ = 0.0063, ε_{Nb} = 0.0100	AV (A = Ca) $\varepsilon_O = \varepsilon'_O$ = 0.0064, ε_{Nb} = 0.0102
Co	2.140	2.408
Nb	5.350	6.014
A1	1.767	1.389
*A*2	1.769	1.387
O1	2.004	2.058
O2	2.022	2.071

(Note that we have adjusted the $\varepsilon_{Nb}/\varepsilon_O$ ratio in this case not to minimize the above functional but to ensure that the Co and Nb ions are equally over-bonded in percentage terms and to equalize as far as possible the AVs of the two independent O ions.) Such a situation is then tailor-made for octahedral rotation in that such rotations automatically expand the size of the CoO_6 and NbO_6 octahedra (thereby reducing the initial over-bonding of the Co and Nb ions) while simultaneously contracting the Sr co-ordination polyhedra (thereby reducing the initial under-bonding of the Sr ions).

In the A = Ca case, using $a_h = b_h \sim 5.5498$, $c_h \sim 6.7203$ Å (derived from the above-refined monoclinic cell dimensions) and choosing ε_O ($= \varepsilon'_O$) = 0.0064 and $\varepsilon_{Nb} = 0.0102$ gives 20.4% over-bonded Co and Nb ions, 30.6% under-bonded Ca ions and O ions that are ~3–4% over-bonded (see column 3 of Table 2). Such a situation is again tailor-made for octahedral rotation, the only real difference between the A = Sr and Ca cases being that one could expect a rather larger amplitude of rotation in the latter A = Ca case. The question now becomes around which axes do the expected octahedral rotations take place?

For cubic perovskite-related phases, it is well-known that octahedral rotation (around $\langle 001 \rangle_p$) modes can only be associated with modulation wave-vectors of the type $\langle \frac{1}{2}, \frac{1}{2}, \xi \rangle^*_p$, etc. [23]. In the current context, where $\mathbf{a}_m = [\bar{1}10]_h = [\bar{1}\bar{1}2]_p$; $\mathbf{b}_m = [\bar{1}\bar{1}0]_h = [1\bar{1}0]_p$; $\mathbf{c}_m = [1\bar{1}2]_h = 3[110]_p$ and $\mathbf{a}^*_m = \frac{1}{2}[\bar{1}11]^*_h = \frac{1}{2}[001]^*_p$; $\mathbf{b}^*_m = \frac{1}{2}[\bar{1}\bar{1}0]^*_h = \frac{1}{2}[1\bar{1}0]^*_p$; $\mathbf{c}^*_m = \frac{1}{2}[001]^*_h = \frac{1}{6}[111]^*_p$, there exist two non-equivalent modulation wave-vectors of this type: $\mathbf{q}_1 = \frac{1}{2}[\bar{1}10]^*_p (\equiv \frac{1}{2}[110]^*_p) = \frac{1}{2}[110]^*_h = -\mathbf{b}^*_m$ and $\mathbf{q}_2 = \frac{1}{2}[111]^*_p = \frac{3}{2}[001]^*_h = 3\mathbf{c}^*_m$ (see Figs. 4 and 5). Octahedral rotation around $[001]_p \equiv [\bar{1}11]_h$ can only be associated with the former modulation wave-vector. The rotation axis in the latter case is, in principle, indeterminate because a $\mathbf{q}_2 = \frac{1}{2}[111]^*_p = \frac{3}{2}[001]^*_h$ modulation wave-vector is compatible with octahedral rotation around any of the three $\langle 001 \rangle_p$ axes or any linear combination thereof [23]. The c glide perpendicular to $\mathbf{b}_m$ in the resultant space group (see Fig. 4c), however, is only compatible with octahedral rotation around $[110]_p$ ($\equiv \frac{1}{3}[1\bar{1}2]_h$) for $\mathbf{q}_2$. Likewise, this c glide constrains the octahedral rotation associated with $\mathbf{q}_1$ to be around $[001]_p$, as expected. In the notation of Glazer et al. [23], the octahedral tilt sequence can therefore only be $b^-b^-c^+$. Such an octahedral tilt sequence is the most commonly observed tilt sequence not only for simple ABO_3 perovskites [23,24] but also for elpasolite-type double perovskites [25] and, judging from this paper and Refs. [3,13], also for 1:2 B site ordered triple perovskites.

Using a modulation wave approach (see, e.g., Ref. [26]), and on the assumption that the symmetry lowering from trigonal $P\bar{3}m1$ to monoclinic $P12_1/c1$ is purely associated with octahedral rotation associated with the two modulation wave-vectors $\mathbf{q}_1$ and $\mathbf{q}_2$, resultant fractional co-ordinates for the 16 independent ions per resultant supercell have been derived as given in Table 3. Fractional co-ordinates are given both with respect to the resultant monoclinic supercell $(x', y', z')_m$ (on the right-hand side of Table 3) as well as the trigonal parent structure $(xyz)_h$ (on the left-hand side of the Table). The relationship between the two is given by $(x', y', z') = (\frac{1}{2}[-x + y + z], \frac{1}{2}[-x - y], \frac{1}{2}[z])$. Note that the four parameters associated with the trigonal intermediate parent structure are again present as are two additional parameters, ε_z (representing the amplitude of octahedral rotation around the $[001]_p \equiv [\bar{1}11]_h$ axis) and ε_{110} (representing the amplitude of octahedral rotation around the $[110]_p \equiv \frac{1}{3}[1\bar{1}2]_h$ axis).

In order to maintain octahedral regularity, i.e., in order for the local octahedral rotation axis to be around a $\langle 111 \rangle_p$ axis, it is necessary for $|\varepsilon_{110}| = 2|\varepsilon_z|$. We have thus assumed that $\varepsilon_{110} = 2\varepsilon_z = 2\varepsilon_R$ (the relative signs of ε_z and ε_R can be freely chosen as they can be changed simply by an origin shift) and that $\varepsilon'_O = \varepsilon_O$, $\varepsilon_A = 0$. With these additional assumptions, the resultant fractional co-ordinates within the resultant monoclinic supercell can then be expressed in terms of only three variables, ε_O, ε_{Nb} and ε_R ($= \varepsilon_{110} = 2\varepsilon_z$) (see Table 4). (Note that 14 out of the 16 crystallographically independent ions in Table 4 are on the general 4*e* position of the space group $P2_1/c$. There are thus $14 \times 3 = 42$ nominally independent fractional co-ordinates to be determined from the formal crystallographic point of view.) Given that $\varepsilon_O \sim 0.0063$ and $\varepsilon_{Nb} \sim 0.0100$ for both A = Sr and Ca (see Table 2), the only parameter remaining to determine is the rotational amplitude parameter ε_R.

Fig. 7 shows a plot of $\Delta(AV)/AV$ for each of the constituent cations as a function of ε_R for both the A = Sr and Ca compounds. In both cases, it can be seen that the Co^{2+} and Nb^{5+} ions are significantly over-bonded and the A^{2+} ions significantly under-bonded without octahedral rotation, i.e., at $\varepsilon_R = 0$. As ε_R increases, the CoO_6 and NbO_6 octahedra simultaneously expand while the A^{2+} co-ordination polyhedra contracts. The initial over-bonding of the Co^{2+} and

Table 3
Modulation wave-derived resultant fractional co-ordinates of the 16 independent ions per resultant monoclinic $P2_1/c1$ supercell given both with respect to the monoclinic supercell itself $(x', y', z')_m$ as well as with respect to the intermediate hexagonal parent structure $(xyz)_h$

Atom	x	y	z	x'	y'	z'
Co_1	0	0	0	0	0	0
Co_2	0	0	1	1/2	0	1/2
Nb_1	1/3	2/3	$2/3+\varepsilon_{Nb}$	$1/2+(1/2)\varepsilon_{Nb}$	$-1/2$	$1/3+(1/2)\varepsilon_{Nb}$
Nb_2	1/3	$-1/3$	$2/3+\varepsilon_{Nb}$	$0+(1/2)\varepsilon_{Nb}$	0	$1/3+(1/2)\varepsilon_{Nb}$
$A1_1$	1/3	2/3	$1/6+\varepsilon_A$	$1/4+(1/2)\varepsilon_A$	$-1/2$	$1/12+(1/2)\varepsilon_A$
$A1_2$	$-2/3$	2/3	$1/6+\varepsilon_A$	$3/4+(1/2)\varepsilon_A$	0	$1/12+(1/2)\varepsilon_A$
$A2$	0	0	1/2	1/4	0	1/4
O11	$1/2+(4/3)\varepsilon_z+(1/3)\varepsilon_{110}$	$0+(2/3)\varepsilon_z-(1/3)\varepsilon_{110}$	$1/2+(2/3)\varepsilon_z-(1/3)\varepsilon_{110}$	$0-(1/2)\varepsilon_{110}$	$-1/4-\varepsilon_z$	$1/4+(1/3)\varepsilon_z-(1/6)\varepsilon_{110}$
O12	$0-(2/3)\varepsilon_z-(1/3)\varepsilon_{110}$	$1/2-(4/3)\varepsilon_z+(1/3)\varepsilon_{110}$	$1/2+(2/3)\varepsilon_z+(1/3)\varepsilon_{110}$	$1/2+(1/2)\varepsilon_{110}$	$-1/4+\varepsilon_z$	$1/4+(1/3)\varepsilon_z+(1/6)\varepsilon_{110}$
O13	$-1/2-\varepsilon_{110}$	$-1/2-\varepsilon_{110}$	1/2	1/4	$1/2+\varepsilon_{110}$	1/4
$O21_1$	$1/6+\varepsilon_O+(4/3)\varepsilon_z+(1/3)\varepsilon_{110}$	$1/3+2\varepsilon_O+(2/3)\varepsilon_z-(1/3)\varepsilon_{110}$	$-1/6-\varepsilon_O'+(2/3)\varepsilon_z-(1/3)\varepsilon_{110}$	$0+(1/2)[\varepsilon_O-\varepsilon_O']-(1/2)\varepsilon_{110}$	$-1/4-(3/2)\varepsilon_O-\varepsilon_z$	$-1/12-(1/2)\varepsilon_O'+(1/3)\varepsilon_z-(1/6)\varepsilon_{110}$
$O21_2$	$-5/6+\varepsilon_O-(4/3)\varepsilon_z+(1/3)\varepsilon_{110}$	$1/3+2\varepsilon_O-(2/3)\varepsilon_z-(1/3)\varepsilon_{110}$	$-1/6-\varepsilon_O'-(2/3)\varepsilon_z-(1/3)\varepsilon_{110}$	$1/2+(1/2)[\varepsilon_O-\varepsilon_O']-(1/2)\varepsilon_{110}$	$1/4-(3/2)\varepsilon_O+\varepsilon_z$	$-1/12-(1/2)\varepsilon_O'-(1/3)\varepsilon_z-(1/6)\varepsilon_{110}$
$O21_3$	$-5/6+\varepsilon_O+(4/3)\varepsilon_z-(1/3)\varepsilon_{110}$	$-2/3+2\varepsilon_O+(2/3)\varepsilon_z+(1/3)\varepsilon_{110}$	$5/6-\varepsilon_O'+(2/3)\varepsilon_z+(1/3)\varepsilon_{110}$	$1/2+(1/2)[\varepsilon_O-\varepsilon_O']+(1/2)\varepsilon_{110}$	$3/4-(3/2)\varepsilon_O-\varepsilon_z$	$5/12-(1/2)\varepsilon_O'+(1/3)\varepsilon_z+(1/6)\varepsilon_{110}$
$O21_4$	$1/6+\varepsilon_O-(4/3)\varepsilon_z-(1/3)\varepsilon_{110}$	$-2/3+2\varepsilon_O-(2/3)\varepsilon_z+(1/3)\varepsilon_{110}$	$5/6-\varepsilon_O'-(2/3)\varepsilon_z+(1/3)\varepsilon_{110}$	$0+(1/2)[\varepsilon_O-\varepsilon_O']+(1/2)\varepsilon_{110}$	$1/4-(3/2)\varepsilon_O+\varepsilon_z$	$5/12-(1/2)\varepsilon_O'-(1/3)\varepsilon_z+(1/6)\varepsilon_{110}$
$O23_1$	$1/6+\varepsilon_O-\varepsilon_{110}$	$-1/6-\varepsilon_O$	$-1/6-\varepsilon_O'$	$-1/4-\varepsilon_O-(1/2)\varepsilon_O'$	$0+\varepsilon_{110}$	$-1/12-(1/2)\varepsilon_O'$
$O23_2$	$-5/6+\varepsilon_O-\varepsilon_{110}$	$-1/6-\varepsilon_O-\varepsilon_{110}$	$-1/6-\varepsilon_O'$	$1/4-\varepsilon_O-(1/2)\varepsilon_O'$	$1/2+\varepsilon_{110}$	$-1/12-(1/2)\varepsilon_O'$

The variable parameters include ε_O ε_O', ε_A, ε_{Nb}, ε_z (representing the amplitude of octahedral rotation around the $[001]_p \equiv [\bar{1}11]_h$ axis) and ε_{110} (representing the amplitude of octahedral rotation around the $[110]_p \equiv \frac{1}{3}[1\bar{1}2]_h$ axis).

Table 4
Modulation wave-predicted resultant fractional co-ordinates of the 16 independent ions per resultant monoclinic $P2_1/c1$ supercell of the A = Sr and Ca compounds given as a function of ε_O ε_{Nb} and ε_R on the assumption (see Table 3 above) that $\varepsilon_{110} = 2\varepsilon_z = 2\varepsilon_R$ and that $\varepsilon'_O = \varepsilon_O$ and $\varepsilon_A = 0$

Atom	x'	y'	z'
Co_1	0	0	0
Co_2	1/2	0	1/2
Nb_1	$1/2+(1/2)\varepsilon_{Nb}$	$-1/2$	$1/3+(1/2)\varepsilon_{Nb}$
Nb_2	$0+(1/2)\varepsilon_{Nb}$	0	$1/3+(1/2)\varepsilon_{Nb}$
$A1_1$	1/4	$-1/2$	1/12
$A1_2$	3/4	0	1/12
$A2$	1/4	0	1/4
O11	$0-\varepsilon_R$	$-1/4-\varepsilon_R$	1/4
O12	$1/2+\varepsilon_R$	$-1/4+\varepsilon_R$	$1/4+(2/3)\varepsilon_R$
O13	1/4	$1/2+2\varepsilon_R$	1/4
$O21_1$	$0-\varepsilon_R$	$-1/4-(3/2)\varepsilon_O-\varepsilon_R$	$-1/12-(1/2)\varepsilon_O$
$O21_2$	$1/2-\varepsilon_R$	$1/4-(3/2)\varepsilon_O+\varepsilon_R$	$-1/12-(1/2)\varepsilon_O-(2/3)\varepsilon_R$
$O21_3$	$1/2+\varepsilon_R$	$3/4-(3/2)\varepsilon_O-\varepsilon_R$	$5/12-(1/2)\varepsilon_O+(2/3)\varepsilon_R$
$O21_4$	$0+\varepsilon_R$	$1/4-(3/2)\varepsilon_O+\varepsilon_R$	$5/12-(1/2)\varepsilon_O$
$O23_1$	$-1/4-(3/2)\varepsilon_O$	$0+2\varepsilon_R$	$-1/12-(1/2)\varepsilon_O$
$O23_2$	$1/4-(3/2)\varepsilon_O$	$1/2+2\varepsilon_R$	$-1/12-(1/2)\varepsilon_O$

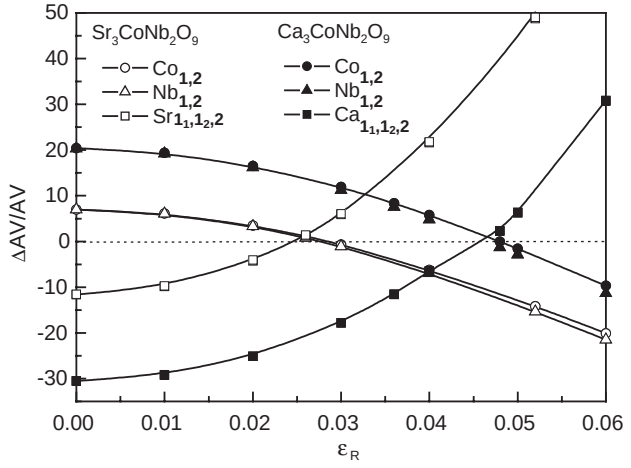

Fig. 7. $\Delta(AV)/AV$ for each of the constituent cations of the resultant monoclinic superstructure as a function of the octahedral rotation amplitude ε_R for both the A = Sr and Ca compounds using the fractional co-ordinates listed in Table 4, the monoclinic cell dimensions listed in the XRPD section and assuming that ε_O $(=\varepsilon'_O) \sim 0.00627$ and $\varepsilon_{Nb} \sim 0.0100$ in the case of the A = Sr compound and ε_O $(=\varepsilon'_O) \sim 0.0064$ and $\varepsilon_{Nb} \sim 0.0102$ in the case of the A = Ca compound.

Nb^{5+} ions thus systematically reduces as does the under-bonding of the A^{2+} ions until each of the $\Delta(AV)/AV$ curves cross the ideal zero position almost simultaneously at $\varepsilon_R = 0.026$ (≡an octahedral rotation around **c** of $\theta_z \sim 5.96°$ and around $[110]_p$ of $\theta_{110} \sim 5.96\sqrt{2} = 8.43°$) in the case of the A = Sr compound and at $\varepsilon_R = 0.048$ (≡an octahedral rotation around **c** of $\theta_z \sim 11.00°$ and around $[110]_p$ of $\theta_{110} \sim 11.00\sqrt{2} = 15.56°$) in the case of the A = Ca

Table 5
Calculated AVs (column 2) for the 16 independent ions of the predicted monoclinic $P2_1/c$, $Sr_3CoNb_2O_9$ structure

Atom label	Calculated result ($\varepsilon_O = \varepsilon_O' = 0.0063$, $\varepsilon_{Nb} = 0.0090$, $\varepsilon_R = 0.026$)			
	AV	Fractional co-ordinates		
		x	y	z
Co_1	2.024	0.0000	0.0000	0.0000
Co_2	2.023	0.5000	0.0000	0.5000
Nb_1	5.040	0.5050	0.5000	0.3383
Nb_2	5.040	0.0050	0.0000	0.3383
$Sr1_1$	2.026	0.2500	0.5000	0.0833
$Sr1_2$	2.025	0.7500	0.0000	0.0833
Sr2	2.028	0.2500	0.0000	0.2500
O11	2.013	0.9740	0.7240	0.2500
O12	2.012	0.5260	0.7760	0.2673
O13	2.013	0.2500	0.5520	0.2500
$O21_1$	2.025	0.9740	0.7146	0.9135
$O21_2$	2.001	0.4740	0.2666	0.8962
$O21_3$	2.045	0.5260	0.7146	0.4309
$O21_4$	2.025	0.0260	0.2666	0.4135
$O23_1$	2.025	0.7406	0.0520	0.9135
$O23_2$	2.025	0.2406	0.5520	0.9135

The predicted fractional co-ordinates (corresponding to the parameter choices $\varepsilon_O = \varepsilon_O' = 0.0063$, $\varepsilon_{Nb} = 0.0100$, $\varepsilon_R = 0.026$; see Table 4) are given in columns 3–5.

Table 6
Calculated AVs (column 2) for the 16 independent ions of the predicted monoclinic $P2_1/c$, $Ca_3CoNb_2O_9$ structure

Atom label	Calculated result ($\varepsilon_O = \varepsilon_O' = 0.0064$, $\varepsilon_{Nb} = 0.0102$, $\varepsilon_R = 0.048$)			
	AV	Fractional co-ordinates		
		x	y	z
Co_1	2.000	0.0000	0.0000	0.0000
Co_2	1.999	0.5000	0.0000	0.5000
Nb_1	4.937	0.5051	0.5000	0.3385
Nb_2	4.934	0.0051	0.0000	0.3385
$Ca1_1$	2.047	0.2500	0.5000	0.0833
$Ca1_2$	2.045	0.7500	0.0000	0.0833
Ca2	2.045	0.2500	0.0000	0.2500
O11	2.005	0.9520	0.7020	0.2500
O12	2.004	0.5480	0.7980	0.2820
O13	1.999	0.2500	0.5960	0.2500
$O21_1$	2.017	0.9520	0.6924	0.9135
$O21_2$	1.944	0.4520	0.2884	0.8815
$O21_3$	2.059	0.5480	0.6924	0.4455
$O21_4$	1.983	0.0480	0.2884	0.4135
$O23_1$	1.998	0.7404	0.0960	0.9135
$O23_2$	1.998	0.2404	0.5960	0.9135

The predicted fractional co-ordinates (corresponding to the parameter choices $\varepsilon_O = \varepsilon_O' = 0.0064$, $\varepsilon_{Nb} = 0.0102$, $\varepsilon_R = 0.048$; see Table 4) are given in columns 3–5.

compound. At this point, all ions are essentially happily bonded in both cases (no AVs differ by more than a few % from their nominally ideal AVs—see Tables 5 and 6). The predicted ($\varepsilon_0 = 0.0064$, $\varepsilon_{Nb} = 0.0102$, $\varepsilon_R = 0.048$) $Ca_3CoNb_2O_9$ compound is shown in projection down the resultant b_m axis in Fig. 8. Note that alternate (100) planes of octahedra rotate around different local $\langle 111 \rangle_p$ rotation axes.

Substitution of these bond valence sum determined values for ε_R, ε_O and ε_{Nb} into the general expressions given in Table 4 for the resultant fractional co-ordinates should thus lead to a pretty good zeroth-order approximation to the resultant structures of both the A = Sr and Ca compounds (see columns 3–5 of Tables 5 and 6). These predicted fractional co-ordinates cannot, however, be expected to be perfect as a result of the approximations inherent in the above bond valence sum analysis—in particular, we have used a small rotation amplitude approximation which is clearly not strictly valid, particularly in the case of the A = Ca compound. Rietveld refinement of high-quality diffraction data (preferably neutron diffraction data in order to enhance the refinability of the O ion positions) is thus still needed in order to precisely refine the $P12_1/c1$ crystal structures of these A = Sr and Ca double perovskite compounds, particularly given the 42 nominally independent fractional co-ordinates to be determined from the formal crystallographic point of view.

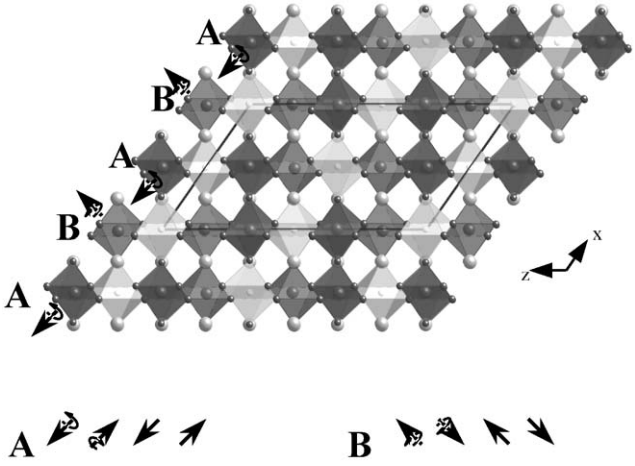

Fig. 8. The predicted ($\varepsilon_O = 0.0064$, $\varepsilon_{Nb} = 0.0102$, $\varepsilon_R = 0.048$) $Ca_3CoNb_2O_9$ compound is shown in projection down the resultant b_m axis. Note that alternate (100) planes of octahedra (labelled A and B) rotate around different local $\langle 111 \rangle_p$ rotation axes (represented by the arrows). The sense of rotation around these local $\langle 111 \rangle_p$ rotation axes is represented by the curved arrows.

References

[1] L.E. Cross, Ferroelectrics 76 (1987) 241–267.
[2] P.K. Davies, Curr. Opin. Solid State Mater. Sci. 4 (1999) 467–471.
[3] I. Levin, L.A. Bendersky, J.P. Cline, R.S. Roth, T.A. Vanderah, J. Solid State Chem. 150 (2000) 43–61.

[4] C.-C. Chou, D.-S. Tsai, I.N. Lin, J. Steeds, Mater. Chem. Phys. 79 (2003) 218–221.
[5] M. Thirumal, A.K. Ganguli, Prog. Crystal Growth Charact. 44 (2002) 147–154.
[6] H. Matsumoto, H. Tamura, K. Wakino, Jpn. J. Appl. Phys. 30 (1991) 2347–2349.
[7] J. Yin, Z. Zou, J. Ye, J. Phys. Chem. B 107 (2003) 4936–4941.
[8] I.G. Siny, R. Tao, R.S. Katiyar, R. Guo, A.S. Bhalla, J. Phys. Chem. Solids 59 (1998) 181–195.
[9] I. Levin, J.Y. Chan, R.G. Geyer, J.E. Maslar, T.A. Vanderah, J. Solid State Chem. 156 (2001) 122–134.
[10] P.K. Davies, J. Tong, T. Negas, J. Am. Ceram. Soc. 80 (1997) 1727–1740.
[11] M.A. Akbas, P.K. Davies, J. Am. Ceram. Soc. 81 (1998) 670–676.
[12] H. Tamura, T. Konoike, Y. Sakabe, K. Wakino, J. Am. Ceram. Soc. 67 (1984) C59–C61.
[13] A.Y. Borisevich, P.K. Davies, J. Solid State Chem. 170 (2003) 198–201.
[14] F. Galasso, J.R. Barrante, L. Katz, J. Am. Chem. Soc. 83 (1961) 2830–2832.
[15] F. Galasso, J. Pyle, J. Phys. Chem. 67 (1963) 1561–1562.
[16] U. Treiber, S. Kemmler-Sack, J. Solid State Chem. 43 (1982) 51–62.
[17] N.E. Brese, M. O'Keeffe, Acta Crystallogr. B 47 (1991) 192–198.
[18] J. Gjønnes, A.F. Moodie, Acta Crystallogr. 19 (1965) 65–67.
[19] M. Bieringer, S.M. Moussa, L.D. Noailles, A. Burrows, C.J. Kiely, M.J. Rosseinsky, R.M. Ibberson, Chem. Mater. 15 (2003) 586–597.
[20] A.J. Jacobson, B.M. Collins, B.E.F. Fender, Acta Crystallogr. B 32 (1976) 1083–1087.
[21] V.S. Urusov, I.P. Orlov, Crystallogr. Rep. 44 (1999) 736–760.
[22] M.W Lufaso, P.M. Woodward, Acta Crystallogr. B 57 (2001) 725–738.
[23] A.M. Glazer, Acta Crystallogr. B 28 (1972) 3384–3392.
[24] C.J. Howard, H.T. Stokes, Acta Crystallogr. B 54 (1998) 782–789.
[25] M.T. Anderson, K.B. Greenwood, G.A. Taylor, K.R. Poeppelmeier, Prog. Solid State Chem. 22 (1993) 197–233.
[26] R.L. Withers, J.G. Thompson, A. Melnitchenko, S.R. Palethorpe, Acta Crystallogr. B 54 (1998) 547–557.